CHAPTER-3

*PIC Simulation of S-Band MILO and Study of Efficiency Enhancement Techniques**

*Part of this work has been published as:

1. **V Nallasamy**, S K Datta, SUM Reddy, and P.K.Jain, "Analysis, Design and Simulation of Metal PBG Waveguide", *International Journal of Microwave and Optical Technology(IJMOT)*, vol.11, no.5, pp.324-331, Sep. 2016.

3.1. Introduction

MILO is a GW-class cylindrical crossed-field oscillator invented by Lemke and Clark in 1987, and became popular for its potential as a high-power microwave (HPM) source for military applications as shown in Fig. 3.1. It has a unique magnetic self-insulating property that enables the tube to handle extremely large input power (tens to hundreds of GW) at a modest applied voltage (several hundred kilovolts). It does not require any externally applied DC magnetic field, which allows the conceptualization of a compact and light weight HPM source. At high voltages, electrons are emitted from the cathode but the current carried by the body (anode) creates a sufficiently strong magnetic field such that these electrons cannot cross the interaction gap. The electrons drift axially in the crossed electric and self-generated magnetic fields. The slow-wave structure (SWS) facilitates the interaction between the axially drifting electrons (the region adjacent to the cathode) and the axially directed slow electromagnetic wave to generate microwaves. However, it suffers from the fundamental limitation of low RF conversion efficiency. This is due to the utilization of maximum load current for generating the self-magnetic field [Lemke *et al*. (1987)].

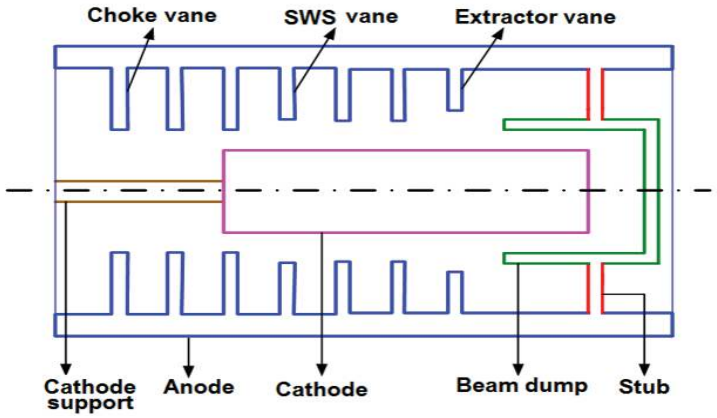

Fig. 3.1: Schematic of MILO.

In the preceding chapter, Chapter 2, the cross field theory applicable to MILO and design methodology approach to conventional MILO has been described. The electron-

beam and RF wave interaction phenomenon in an arbitrary interaction circuits is rather intricate as there are number of parameters which will influence the overall performance of the device. Based on the analyses, computer codes developed and their validity has been benchmarked with the literature results. The design parameters of this MILO are optimized and validated with the published conventional MILO [Cousin *et al*. (2006)]. Of course, the well established cross field theory provides a comprehensive scenario of beam-wave interaction mechanism in MILO. Simultaneously, the particle-in-cell (PIC) simulation codes have also being used in order to investigate the beam-wave interaction phenomenon in high power microwave (HPM) devices including slow wave MILO, Reltron, Vircator, Relativistic Backward Wave Oscillators (RBWO), fast-wave devices like Gyrotron, etc. [Benford *et al*. (2016)]. The PIC simulation helps us to have an in-depth understanding of the EM behavior of the device. This also validates and helps in optimizing the design parameters and the device performance can be observed to realize more reasonable circumstances by integrating various practical constraints easily.

The MILO uses the co-axial type cylindrical cavities as its RF interaction circuit. The RF interaction circuit is cold (in absence of the electron beam) simulated for its EM behavior for confirming the desired operating mode and its dispersion characteristics. The real performance of the MILO could be realized under practical condition, i.e., under hot condition (in the presence of the electron beam) using a commercially available advanced 3D PIC codes, like, MAGIC, MAFIA, CST Studio Suite, etc. These codes basically provide a thorough understanding of the complex beam-wave interaction process in any vacuum electron devices. Kory has presented the 3-D PIC simulation module of MAFIA for investigating a helix TWT interaction mechanism [Kory (2001)]. The PIC module of CST Particle Studio was used for the designing of 650 GHz helical BWO [Kory and Dayton (2009)].

In order to study the reliability and accuracy of "CST PIC simulation code" and its efficient use in HPM device like MILO using conventional RF interaction circuits, the RF behavior of S-band MILO using a co-axial cylindrical cavity type slow-wave structure (SWS) in this chapter is presented. The MAGIC simulation code was also used to investigate the RF behavior of MILO [Cousin *et al*. (2006)], however, in the present work, a 3D PIC code called "CST particle studio" is reconfigured for the MILO electrical and physical structure. The PIC solver module of "CST particle studio" is used to investigate the beam-wave interaction mechanism [CST user's manual (2015)].

In CST particle studio code, the presence of all modes in the SWS of MILO could be observed in terms of signal amplitudes which provide a more reasonable scenario. The field values are recorded in the time domain and its Fourier transform provides the device frequency of operation. The electron particle beamlets at different time intervals within one cycle are shown to understand the bunching mechanism. The energy distribution of all the particles along the interaction length is demonstrated to understand the energy transfer phenomena. Beam-wave interaction yields the temporal RF power growth at the output end of the interaction structure. The stability of the device is also discussed.

In this chapter, the design and simulation of an S-band MILO is presented to improve its overall efficiency by reducing the total length and proper impedance matching at the output by using stubs. The rest of the chapter is organized as follows: In section 3.2, the basic description of "Numerical Techniques" and its features are discussed. The analytical design methodology and the dispersion of MILO are presented in Section 3.3. The 3D modeling and PIC simulation of the improved MILO are narrated in Section 3.4. The technique of efficiency enhancement is briefed in Section 3.5 and the conclusions are drawn in Section 3.6.

3.2. Description of Numerical Techniques

Numerical techniques have made the modernization in the field of electromagnetic applications. In the present era, the design and analysis of electromagnetic problems needs consistent, precise and flexible simulation tools. Computer techniques for investigating the electromagnetic problems fall into one of three categories, analytical methods, numerical methods, and expert systems. Analytical methods are suitable for uniform and simple geometries. Numerical methods can be applied for complex and heterogeneous geometries. Expert systems do not actually calculate the field directly, but instead estimate values for the parameters of interest. Numerical techniques require more computation than other two methods but they are powerful simulation tools. There are numerous numerical techniques available for solving electromagnetic problems and each method is well suited for the analysis of a particular type of problem and a variety of numerical techniques are being used for the beam-wave interaction calculation. The most widely used to techniques are the finite-difference-time-domain (FDTD) method, the finite integration technique (FIT), the finite-element method (FEM), and the method of moments (MoM). The FIT method has been used for applications over an extremely wide range of frequencies, from DC to THz.

The "CST Microwave Studio" is a general purpose electromagnetic simulator based on the finite integration technique (FIT) and which was first proposed by Weiland in 1977. This numerical method provides a universal spatial discretization scheme, applicable to various electromagnetic problems, ranging from static field calculations to high frequency applications in time or frequency domain. Unlike most numerical methods, FIT discretizes the integral form of Maxwell's equations, rather than the differential one. In order to solve these equations numerically a finite calculation domain is defined, enclosing the considered application problem. By creating a suitable

mesh system, this domain is split up into several small cuboids, so called grid cells [Ragha and Bhatia (2007)].

This first or primary mesh can be visualized in the mesh view [CST user manual (2015)]; however, internally a second or dual mesh is set up orthogonally to the first one. The spatial discretization of Maxwell's equations is finally performed on these two orthogonal grid systems. The FIT belongs to the class of local approach in the sense, that the discrete equations are derived cell- by-cell by transforming the continuous Maxwell's equations on to the computational grid. Other representatives of local approaches are Finite Differences (FD), Finite Volumes (FV), Finite Elements (FE), and the Cell Method (CM). All these approaches are based on a volume discretization, defined by the three-dimensional mesh.

The FIT based CST particle studio is a 3-D electromagnetic simulation tool and which has been extensively used for studying the beam wave interaction mechanism in most of the electron beam devices due to the simple and efficient algorithm. It has also been well suited to these applications because it can efficiently model the heterogeneous geometries. The CST PIC studio uses the hexahedral/tetrahedral meshing technique for discretizing the computational domain and which is also more user friendly interface for analyzing results with its post-processing module. Another PIC code is MAGIC and which is a user configurable one based on FDTD method. This tool calculates only one mode (desired operating mode) at a time but the CST particle studio calculates the multiple modes (desired and competing) simultaneously and which is a GUI based 3-D simulation code

The salient features of "CST Microwave studio" are its diagnosis of results and post-processing module. It provides users to employ six different field solvers, electrostatic, magneto-static, Eigen mode solver, particle tracking solver, particle in cell solver (PIC)

and wake- field solver. In cases of strongly resonant loss-free structures, where the fields (the modes) are to be calculated, the Eigen mode solver is very efficient. The Eigen mode solver cannot be used with open boundaries or discrete ports [CST user's manual (2015)]. Magneto-static solver can be used for static magnetic problems while Electrostatic solver can be used for static electric problems. Both of these solvers utilizes feature of open boundary conditions. These help to reduce the number of mesh nodes, when problems in free space are simulated. The gun and particle tracking solver can be used to compute trajectories of charged particles within electrostatic, magneto-static or Eigen mode fields. A self-consistent electrostatic field is calculated using gun-iteration implemented which considers the reaction of the particle movement to the electrostatic potential distribution. Particle sources can be defined at arbitrary surface of solids that emits particles according to the predefined emission models. The major task for the trekking solver is to calculate the particle trajectories, the self-consistent electrostatic field, the space charge distribution and the particles' current. These results appear automatically in the navigation tree after the solver run. The particle tracking solver also offers the tracking of different types of particle from different sources independently. Thus, multi-beam guns or the parallel simulation of particle beams can be simulated. The computation of wake-potentials of charged particle bunches can be performed using the wake-field solver. For the designing of particle-accelerators, wake-potentials provide important information. The PIC solver simulates the evolution of charged particles in self-consistent electromagnetic fields. Moreover, in the PIC simulation, the static or analytic field distributions can easily be added. Feature of PIC solver includes the charged particles emission from arbitrary surfaces or single points. Like other PIC codes, CST Particle Studio also involves four major steps before proceeding for the solution of beam-wave interaction problems. The basic steps in the

particle simulation (beam present simulation) of RF interaction circuit using PIC solver are described below.

In the CST particle studio, initially, the 3-D electromagnetic circuit has to be defined with the required specifications. In the present problem, a conventional co-axial cylindrical type SWS as an RF circuit is chosen and its specifications are given in Table 3.1. For the beam absent analysis, the electromagnetic circuit is simulated using an Eigen mode solver of the CST microwave studio. In the 'quick start guide' of the software code for the corresponding relevant solver module, the important steps can be determined. After defining the geometry, simulation frequency range of simulation should be defined as per the operating region of the electromagnetic circuit. A port is defined at the output section of circuit in order to determine the signal amplitude corresponding to different modes.

A desired cross section of an electron beam is injected into the electromagnetic structure, in order to make the interaction between the beam and the RF signal. The dimension of the beam is decided according to the circuit dimension and the desired operating mode. The parameters for developing the electron beam are also defined. A suitable electron optic model is chosen for the problem concern. The emission of particles is defined at the flat surface and the angle of tilt is obtained from the ratio of transverse velocity of the beam to the axial velocity, i.e., pitch factor. The cathode has the radius same as that of the beam radius. According to triangular mesh generated in the surface, the emission of particles can be defined as well as controlled. More number of mesh cells can give higher accuracy with higher emission of particles but it requires more computational time and memory. The current must be approached to its peak value, so that the simulation run is stable. Here, the DC beam emission model is taken which requires assigning any of the constant value parameter to the particles as Lorentz

factor (γ), normalized velocity (β), Drift velocity of electrons (v_d), Beam Voltage (V_b). These parameters can be calculated as :

$$\gamma = 1 + eV_b / m_e c^2 , \tag{3.1}$$

$$\beta = \sqrt{1 - 1/\gamma^2} , \tag{3.2}$$

$$v_d = \beta c , \tag{3.3}$$

$$V_b = (\gamma - 1)\ (m_e c^2/e) . \tag{3.4}$$

where, e is charge and m_e is rest mass of the electrons, c is velocity of light, V_b is beam voltage. The monitors of electric and magnetic field as well as power developed in the RF structure are defined in the specified dialog box. Particles are also monitored in 2-D or 3-D planes to have information about perturbation of the particles in terms of energy or phase and bunching phenomena. Using this monitor commands, particles are monitored at a set interval of time over full or partial time of simulation for their momentum, position, etc. A 2-D particle monitor can be set at any of the position in 2-D plane mostly at the saturation position or at the entry plane of the collector to acquire the modulation of energy or momentum among particles.

3.3. Design Methodology

MILO with the slow-wave structure comprising periodically spaced choke cavities and SWS cavities in a smooth waveguide is shown in Fig. 3.2. The slow-wave structure supports number of slow-wave modes. Suitable phase synchronism between any one of these electromagnetic modes and the drifting electrons (with velocity $v_d = E_o /B_o$, where E_o and B_o are the electric field in radial direction and magnetic field in azimuthal direction, respectively) results in efficient conversion of beam energy to RF energy.

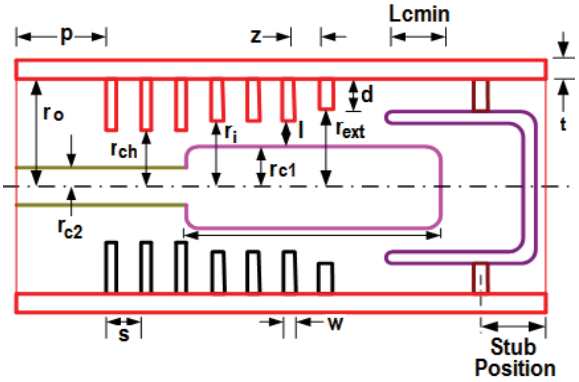

Fig. 3.2. Schematic of MILO with all parameters

Here, r_o and r_i are the outer and inner radii of the SWS vanes; $d(=r_o - r_i)$ is the cavity depth; w is the thickness of the SWS vane; $z(=s-w)$ is the distance between the SWS apertures; r_{c1} is the cathode radius; s is the circuit periodicity. At the beam voltage of 500kV and impedance of 25 Ω, the ratio of the inner radius of the anode to the cathode radius is given by [Cousin (2005)] :

$$\frac{r_i}{r_{c1}} = 1.6 \quad , \tag{3.5}$$

From the practical consideration , the radius of choke vane (r_{ch}) and the radius of cathode support rod (r_{c2}) is lesser than the inner radius of the anode to the cathode radius in order to have smooth impedance transition towards pulse power supply is given by [Cousin (2005)].

The length of the cathode, L_{SE} is arrived from the perveance of the device :

$\mu = I_C / V_o^{3/2}$, given as [Parker *et al.* (1974)] :

$$L_{SE} = 6.82\times10^4 \mu r_i \left(\ln\left(r_i / r_{c1}\right)\right)^2 \quad , \tag{3.6}$$

The design starts with the inputs: the operating frequency (f), beam voltage (V_0), cathode radius (r_{c1})and the width of the SWS vane (w) is chosen with practical considerations

[Lemke *et al*.(1997)], [Nallasamy *et al.* (2016)], [Cousin (2005)]. The values of the circuit periodicity (s) and cavity depth (d), are arrived at using the condition of synchronism ($v_\phi = v_d$) and the expressions (3.1) and (3.2) with the known value of operating frequency (f). The expressions (3.9) and (3.10) are used with the known value of beam voltage (V_0) and (r_i / r_{c1}) from equation (3.5) to arrive at the critical current for self-magnetic insulation and total current in the device for sustainable oscillation. The value of inner radius of the SWS vane (r_i) is directly calculated using (3.5); and the value of outer radius of the SWS (r_o), interaction gap (z) and the free space gap between anode to cathode (l) are obtained from the relations, $r_o = r_i - d$, $z = s - w$ and $l = r_i - r_{c1}$, respectively.

The resonant frequency, ω_o of an individual SWS cavity of the MILO can be expressed in terms of the circuit parameters following equivalent circuit approach as [Fan *et al.* (2008)]:

$$\omega_0 = \left(\frac{\mu_0 z d}{4\pi r_0} \left[2\varepsilon_0 r_i \ln\left(\frac{z/2 + w}{z/2} \right) + \frac{2\pi\varepsilon_0}{3zd} \left(r_0^3 + 2r_i^3 - 3r_0 r_i^2 \right) \right] \right)^{-1/2} , \tag{3.7}$$

where, μ_0 is the permeability of free-space; z is the distance between the SWS apertures; For a slow-wave structure comprised of N number of cavities, the resonance condition would necessitate the following condition to satisfy:

$$2N\varphi = 2k\pi , \tag{3.8}$$

where, N is the number of SWS cavities; k is an integer and φ is the phase difference between the adjacent cavities. The resonant frequency of the coupled cavity stack, ω_{ok} can be now given as [Fan *et al.* (2008)]]:

$$\omega_{0k} = \omega_0 \left(1 + \frac{\dfrac{2\pi\varepsilon_0 w}{\ln\left(r_i / r_{c1}\right)} + 8\varepsilon_0 \left[z + \left(r_i - \dfrac{2l}{\pi} \right) \ln\left(1 + \dfrac{\pi z}{2l} \right) \right]}{2\left[2\varepsilon_0 r_i \ln\left(1 + \dfrac{2w}{z} \right) + \dfrac{2\pi\varepsilon_0}{3zd} \left(r_0^3 + 2r_i^3 - 3r_0 r_i^2 \right) \right]} \left(\frac{1}{1 - \cos\phi} \right) \right)^{-1/2} . \tag{3.9}$$

When cathode current becomes higher than the critical current, the self-magnetic field generated confines the electrons and it does not reach up to the anode. The electrons derive equipotential surfaces and move perpendicular to the crossed electric and magnetic fields. The minimum current or critical current I_{cr} required to insulate the beam is defined as [Dwivedi and Jain (2013)] :

$$\begin{aligned} I_{cr} &= I_0 \sqrt{\gamma_o^2 - 1} / \ln\left(r_i / r_c\right) \\ &= \frac{4\pi m_0 c^3 \varepsilon_o \sqrt{\gamma_o^2 - 1}}{e \ln\left(r_i / r_c\right)} \end{aligned} , \tag{3.10}$$

where, r_c and r_i are the cathode and anode radii, respectively; I_o is the starting current for oscillation, e is the electron charge and m_o is the electron mass at rest; $\gamma_o=(1-\beta^2)^{-1/2}$ is the relativistic mass factor with $\beta=v_d/c$ as the normalized electronic drift velocity with respect to the velocity of electromagnetic wave in free-space as evaluated at the anode. As the insulated electron flow fills the anode-to-cathode gap (A-K-gap), the total anode current or para-potential current, I_p becomes [Dwivedi and Jain (2013)] :

$$I_p = \frac{I_0 \gamma_o \ln\left(\gamma_0 + \sqrt{\gamma_o^2 - 1} \right)}{2 \ln\left(r_i / r_c\right)} . \tag{3.11}$$

Under the condition of Diocotron instability [Chen, (1985)], few of the electrons of the beam reach the anode and few others remain at the magnetic cutoff, while the other electrons migrate towards the anode in bunch form (usually called spokes). The mode of oscillation of MILO is established when electron drift velocity is slightly greater than the phase velocity of the RF wave. The condition of synchronism is given as [Cousin (2005)],

$$v_d = \frac{E_0}{B_0} = \frac{V_0}{2\ln\left(r_i / r_c\right)}\left(\frac{2\pi r}{\mu_0 I_t}\right) = \frac{2\pi\varepsilon_0 c^2}{\ln\left(r_i / r_c\right)}\left(\frac{V_0}{I_t}\right) \cong 0.3c \ , \tag{3.12}$$

where, v_d is the electron drift velocity; ε_o is the permittivity of free-space; I_t is the total anode current. The RF phase velocity, v_φ at which electronic interaction could take place can be now expressed under the condition of synchronism, $v_\varphi \approx v_d$ as [Cousin (2005)] :

$$v_\varphi = \frac{s}{2dc} \cong 0.3c = \frac{\omega}{\beta_0} = \frac{2\pi f}{\left(\pi / s\right)} = 2sf \ , \tag{3.13}$$

where, ω is the angular frequency, s is the periodicity of the slow-wave structure (SWS), d is the vane height, f is the operating frequency, and β_o is the axial propagation constant. In order to complete the design, it would be now required to arrive at the length of the load, the length of the cathode and the efficiency of the device. These parameters are arrived at from the consideration of Hull cut-off and Buneman-Hartree conditions. The cathode current I_c under Hull cut-off criteria is defined as [Cousin (2005)] :

$$I_C = \frac{8500}{\ln\left(r_i / r_c\right)}\left[\frac{eV_H}{m_0c^2}\left(2 + \frac{eV_H}{m_0c^2}\right)\right]^{\frac{1}{2}} \ \ (\textit{Hull cut-off}) \ , \tag{3.14}$$

Here, V_H is the Hull cut-off voltage; e and m_o are the charge and mass of electrons at rest, respectively. The relation between the cathode current, I_c and the Buneman-Hartree voltage, V_{BH} is given by [Cousin (2005)] :

$$I_C = \frac{8500}{\beta_0 \ln\left(r_i / r_c\right)}\left[\frac{eV_{BH}}{m_0c^2}\left(1 - \sqrt{1-\beta^2}\right)\right] \ . \tag{3.15}$$

For a given operating voltage, when the minimum load length is decided at the condition of charging current reaching the value of critical current, I_{cr}. Under such condition, the minimum length of load, $L_{C\,min}$ is defined by [Lemke *et al.* (1997)] :

$$L_{C\min} = 2r_{c1}\ln\left(\frac{r_i}{r_{c1}}\right)\frac{\sqrt{\gamma^2 - 1}}{\left[G\left(\gamma_0\right)\right]^2} \ , \tag{3.16}$$

where, $G(\gamma_0) \approx 2\left(\gamma_0^{1/2} - 0.847\right)$. The length of the cathode, L_{SE} is arrived from the perveance of the device $\mu = I_C / V_o^{3/2}$, given as [Parker *et al.* (1974)] :

$$L_{SE} = 6.82 \times 10^4 \, \mu r_i \left(\ln\left(r_i / r_{c1}\right)\right)^2, \tag{3.17}$$

where, μ is the diode perveance that depends on geometrical parameters, I_c is the cathode current and V_o is the cathode voltage. The corresponding maximum efficiency, η_{max} of the MILO relative to the input beam power is given by [Lemke *et al.* (1997)] :

$$\eta_{\max} = \frac{P_{\max}}{V_0 I_p} = 0.32\left(\frac{I_{s,\max}}{I_p}\right) = 0.32\left[1 - \left(\frac{I_{cr}}{I_p}\right)\right], \tag{3.18}$$

where, $P_{max} = 0.32 * I_{s,max} * V_o$ and $I_{s,max} = I_p - I_{cr}$, is the maximum total dc spoke current, V_o is dc A-K gap voltage, and P_{max} is the corresponding output power of the MILO. The maximum power conversion efficiency is possible to be obtained for the condition of transit angle corresponding to the gap approaching π which is accounted for with the numerical value of 0.32 as given in the equation (3.18). However, both simulations and experiments for a load-limited MILO have shown efficiencies quite close to those predicted by (3.18). Stub position at the end of beam dump and the placement of choke vane (p) are generally kept as $(2n+1)\lambda/4$; where n = 0, 1, 2, 3, …. The radius of extractor vane is decided by trial and error method. The total length of MILO is decided by periodicity, choke cavity, SWS and extractor cavity, length of collector covering the cathode and remaining part of collector.

The region of operation of the proposed device with r_c = 25 mm, r_i = 40 mm, s =13 mm, and $2d$ = 42.8 mm as obtained from the analysis is shown in Fig. 3.3. The dispersion characteristics of the four cavity slow wave structure operating in π-mode at the frequency of 3.3 GHz is shown in Fig. 3.4 as computed using the equivalent circuit analysis. The device operates at a constant voltage within the regime $V_{BH} < V < V_H$ with the electron beam intensity limited by self-generated magnetic field. The Buneman-

Hartree condition does not become prevalent due to the corresponding plot remains below the para-potential current.

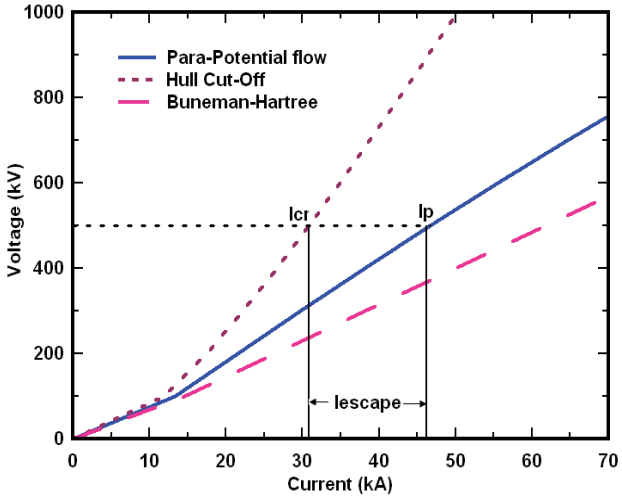

Fig. 3.3: Region of operation of the MILO for r_c= 25 mm, r_i = 40 mm, s=13 mm, 2d = 42.8mm ,w = 4mm

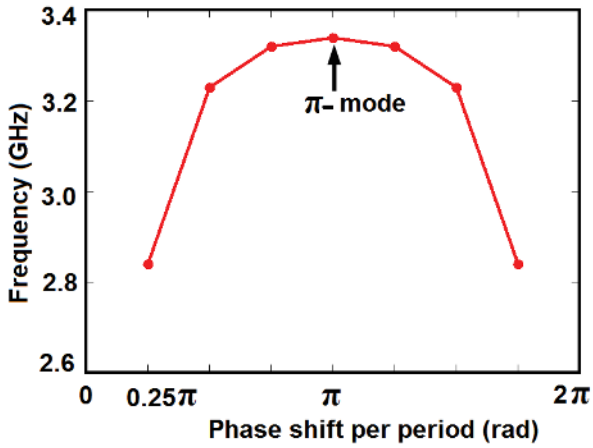

Fig. 3.4: Dispersion characteristics of the four cavity SWS.

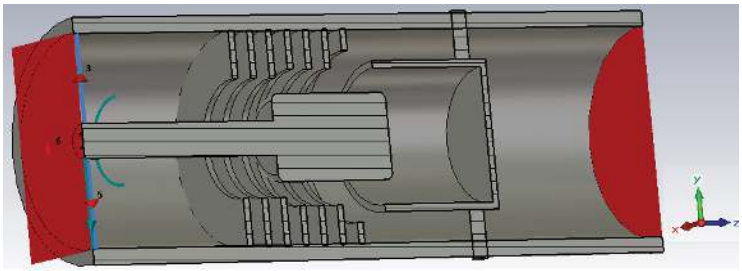

Fig. 3.5: 3D model of the proposed MILO in CST environment.

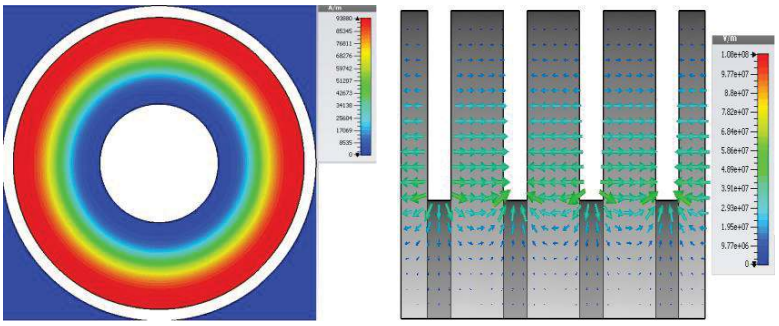

(a) *(b)*

Fig. 3.6: (a) TM_{01} field pattern, and (b) π-mode in SWS of MILO.

3.4. Modeling and Simulation of Conventional MILO

3.4.1. Electron Beam Absent (Cold) Simulation

In our design, the RF section comprises seven vanes: three choke vanes, three SWS vanes, and one extractor vane. The first three vanes (choke vanes) constitute the RF choke cavity that is operated at frequency less than the pi-mode frequency. The dimensions of the next three vanes (SWS vanes) decide the frequency of oscillation as the beam-wave interaction takes place in this region. The inner radius of the last vane (extractor vane) is kept larger than SWS vanes and it plays a vital role in extracting RF energy from the interaction region. The extractor vane and beam dump form the RF extracting cavity. The 3-D modeling of the device was carried out using CST Studio with adaptive mesh refinement. A 3-D schematic of the MILO with short-length cathode is shown in Fig. 3.5. The design parameters used in the present model are shown in Table 3.1. All the vanes including choke, SWS, beam dump, cathode, anode, and stubs of MILO structure have been modeled using a perfect electric conductor (PEC) with background as vacuum. The MILO structure has been modeled and simulated in the linear co-ordinate system using hexahedral meshing. Both electric and magnetic fields satisfy the boundary conditions imposed by the walls of the RF circuit.

The Eigen-mode analysis has been carried out for the desired TM_{01}-mode in the SWS (Fig. 3.6). The *E*-field in adjacent cavities are 180° out of phase which confirms the π-mode of operation at 3.3 GHz. The field distribution associated with π-mode produces the strongest coupling to the electron beam with high Q (quality factor) space-harmonics. To maximize the power output in our improved MILO, four short-circuited stubs are placed at 90 degrees apart that provide return path for electron beam. These are mechanically joined to the extractor and anode for impedance matching and also acting as a short circuit for dc but an open circuit for RF.

Table 3.1: Optimized Design Parameters of MILO.

Parameters	Designed Parameters	Optimized Parameters
SWS vane radius (r_i)	40.0 mm	39.0 mm
Extractor vane radius (r_{ex})	48.0 mm	49.0 mm
Cavity Period (s)	12.9 mm	13.0 mm
Beam dump inner radius	40.0 mm	39.0 mm
Beam Dump outer radius	44.0 mm	43.0 mm
Beam Dump length	164.4 mm	84.4 mm
Cathode projection inside Beam Dump	123.4 mm	7.4 mm
Length of cathode	200.0 mm	80.0mm
Total length of MILO	373.8 mm	289.8 mm

3.4.2. Electron Beam Present (Hot) Simulation

A few assumptions are used for the PIC simulation: the electric and magnetic fields are assumed to be confined to the space within the RF interaction circuit, dielectric loss is negligible, and the power loss at the metallic boundaries is also negligible. For the beam-present simulation, four discrete ports at 90° apart have been defined at the input port of the MILO for applying high voltage between the cathode and the anode. In the RF circuit of MILO, electrons have been considered as uniformly longitudinally

distributed, and their evolution along the axial direction in the presence of RF noise has been monitored in time domain.

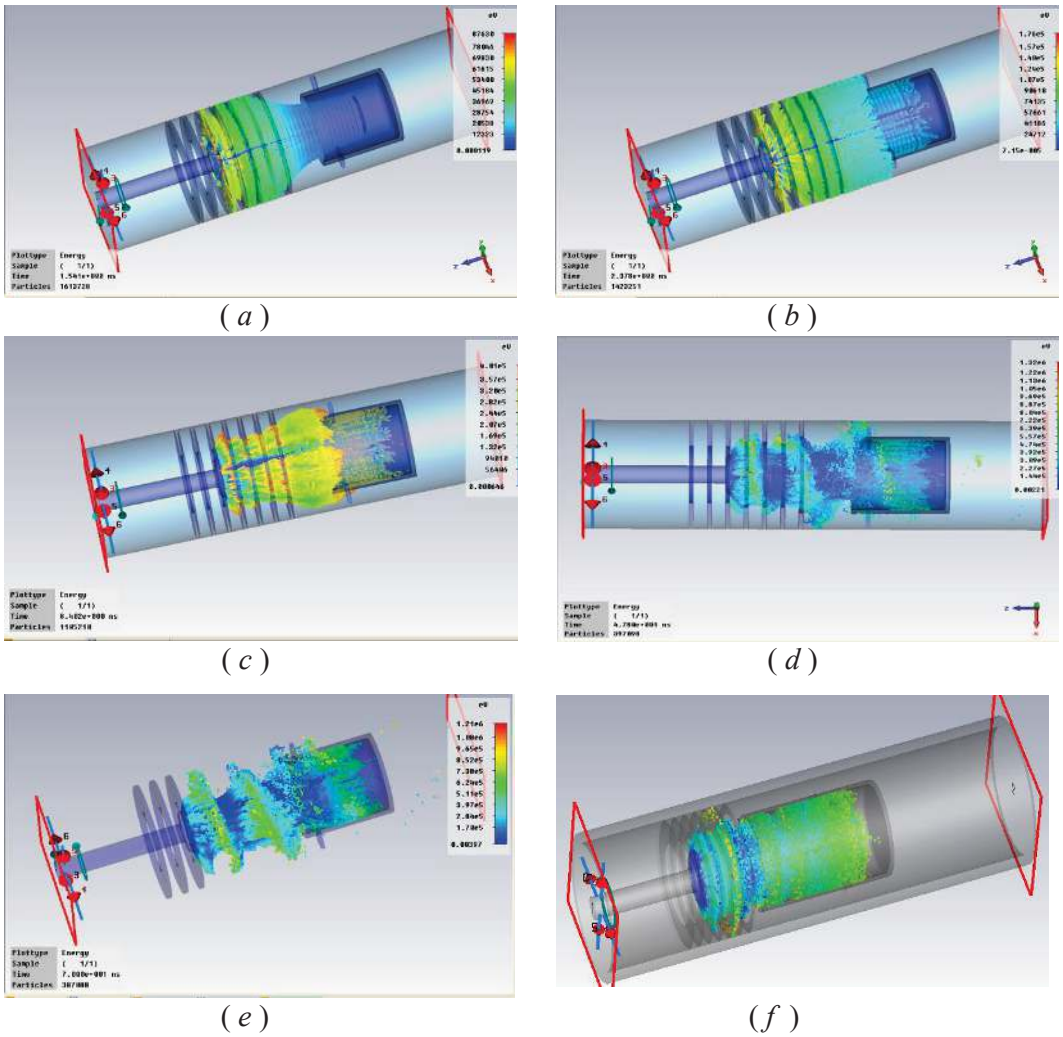

Fig. 3.7 : (*a*) Particle view at 1.5ns (no self-magnetic established) (*b*) Particle view at 2.37ns (no self-magnetic field established) (*c*) Particle view at 8.4ns (self-magnetic field established) (*d*) Particle view at 47.8ns (spokes formation) (*e*) Particle view at 48.5ns (spokes formation) and (*f*) Particle view at 100ns (after rf power extracted from beam power at the end of simulation)

A beam voltage of 500kV with the rise time of 1ns was applied between cathode and anode at the input port to facilitate generation of electron beam due to explosive emission from the surface of a cylindrical velvet cathode. After applying beam voltage, Fig.3.7 (*a*) and Fig.3.7 (*b*) shows that all electrons drift towards anode because no self-

magnetic field is established. Establishment of self magnetic field inside RF interaction structure is shown in Fig.3.7 (*c*) where all electrons are confined to the cathode at t=8.4ns. Due to the self-generated magnetic field, electron beam remains insulated between the SWS vanes and cathode. Spokes formation of electrons is shown in Fig.3.7 (*d*) and Fig.3.7 (*e*) at t = 47.8ns and t = 48.5ns respectively. Particle view at 100ns is shown in Fig.3.7 (*f*) where all electrons are collected in the beam dump after the RF power is extracted from beam power at the end of simulation time at t = 100ns. The electron distribution was observed to be axis-symmetric in each transverse cross section in the *yz*-plane at t = 65.72 ns as shown in Fig. 3.8. In order to observe the growth of the RF field, we set a number of electric field probes. The generation of RF power was monitored at the output port. The impedance discontinuity between the choke vanes and SWS vanes benefitted the MILO operation as the high impedance in the choke vane section resulted in lower E-field to avoid electrical breakdown and the low impedance in SWS vane section resulted in high spoke current. The higher spoke current due to more electrons at the interaction region enhanced the efficiency to ~ 25% as compared to the similar conventional MILOs that offer efficiencies of ~15% [Cousin *et al.* (2007)] and 12% [Qin *et al.* (2012)]. The *E*-field amplitude at the output port was obtained as 80 kV/m (Fig. 3.9). The RF output of ~ 6GW was observed (Fig. 3.10) at 3.1GHz in TM_{01} fundamental mode of operation with beam current of 50 kA and beam voltage of 500 kV (Figs. 3.11 and 3.12). The Fourier transform of *E*-field amplitude shows the desired frequency of operation as 3.1 GHz as shown in Fig 3.13. The magnetic field distribution at the output port (Fig. 3.14) clearly indicates that the improved design operates in fundamental mode. The microwave frequency obtained from the simulation is 3.1 GHz against that of the cold π-mode frequency of 3.3 GHz.

The shift in the simulated operating frequency is attributable to the beam loading effect. The energy distribution over the interaction length at t = 95 ns is shown in Fig. 3.15.

3.5. Efficiency Enhancement Technique for MILO

The enhancement of overall efficiency was obtained by reducing the inner radius of choke vane, SWS vane, Extractor vane and Beam dump by 1mm. In addition to the above the position of stubs on the beam dump played vital role in matching the impedance at the output of MILO in order to extract maximum RF power. A part of the cathode extended into the Beam dump was reduced from 164.4mm to 7.4mm for maintaining the sufficient load length required to generate the critical current for generating the required self-magnetic field and also the reduced cathode length helped in preventing off axis shift due to cantilever force and thus asymmetric emission of electron beam is prevented. In view of the above, the overall efficiency of the Improved MILO is enhanced to 25% for the voltage of 500kV and current of 47.5kA.

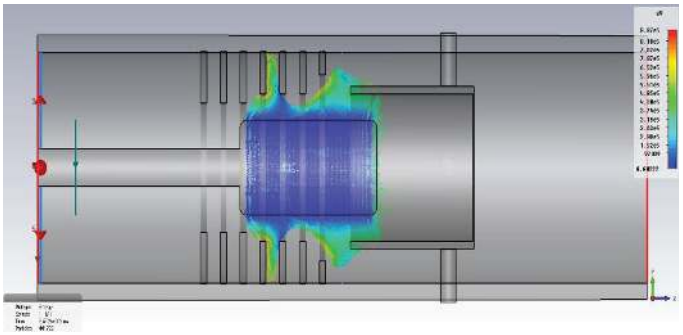

Fig. 3.8 : Distribution of electrons at 65.72 ns.

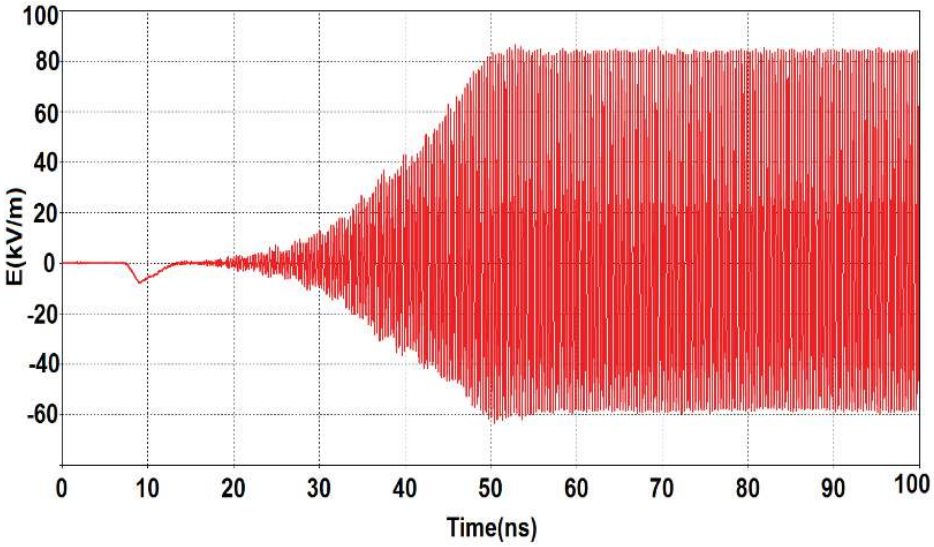

Fig. 3.9 : Instantaneous E-field amplitude.

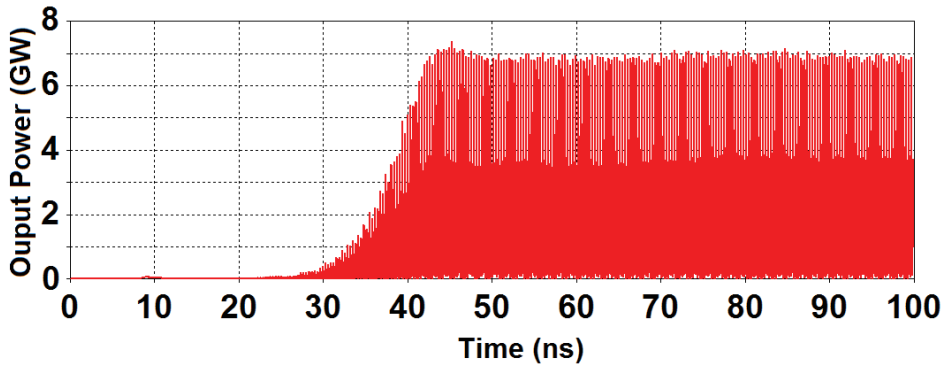

Fig. 3.10 : Peak output power of improved MILO.

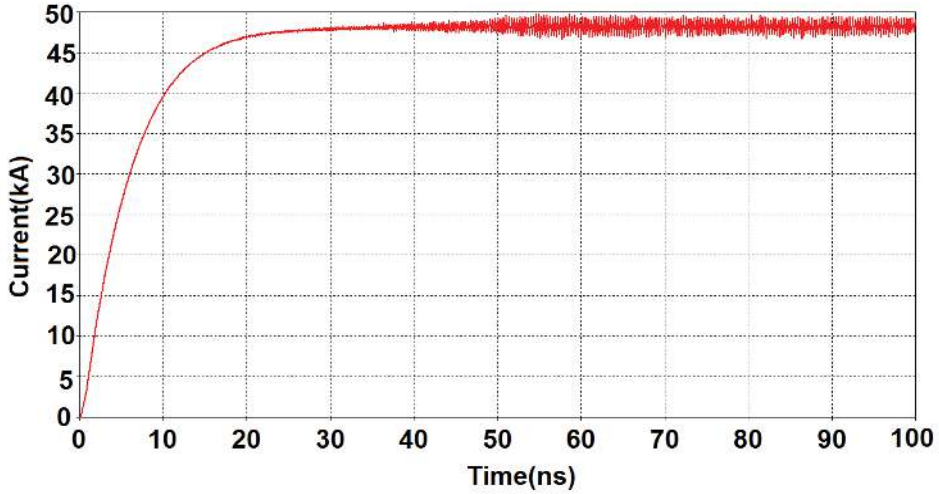

Fig. 3.11 : Build-up of current with time.

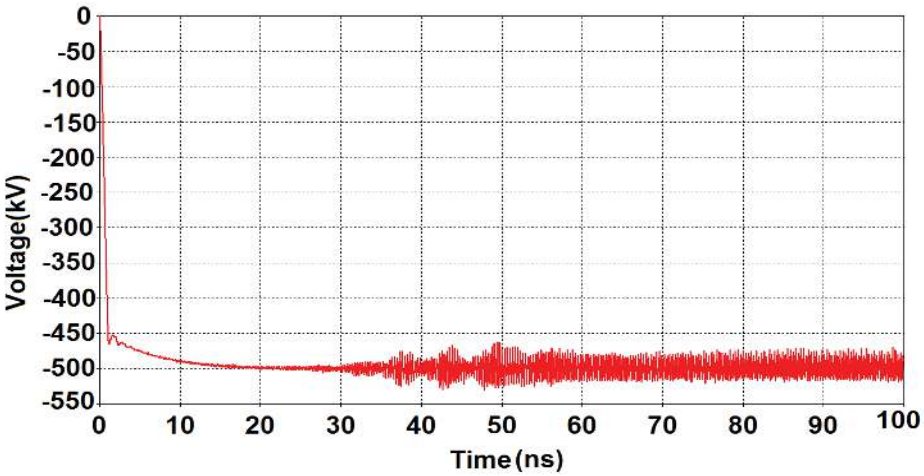

Fig. 3.12 : Build-up of voltage with time.

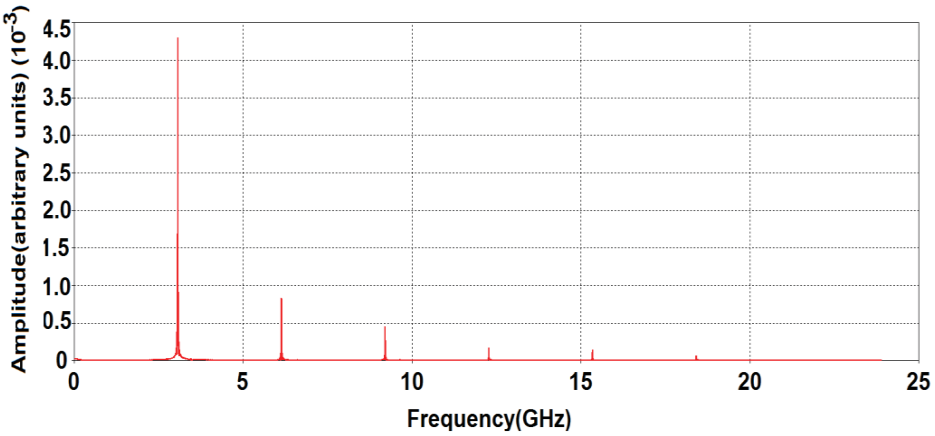

Fig. 3.13 : Fourier transform of the electric field at the output port.

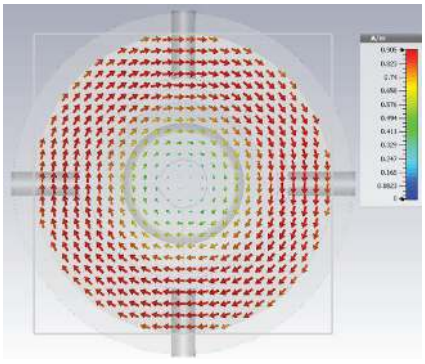

Fig. 3.14 : The TM_{01} magnetic field distribution at the output port.

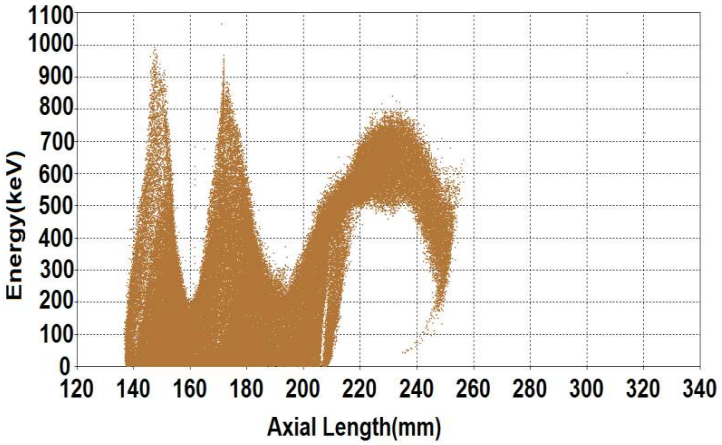

Fig. 3.15 : Energy distribution against interaction length at 95 ns.

Table 3.2: Comparison of results for validation.

Parameters	Results	
	Simulation using MAGIC [Cousin *et al.* (2007)]	Simulation using CST Particle studio
Beam Voltage	500 kV	500 kV
Beam Power	23.5 GW	23.5GW
Frequency	2.44 GHz	2.48GHz
RF Output Power	2.5 GW	2.54 GW
Power Conversion Efficiency	10.6 %	10.8 %

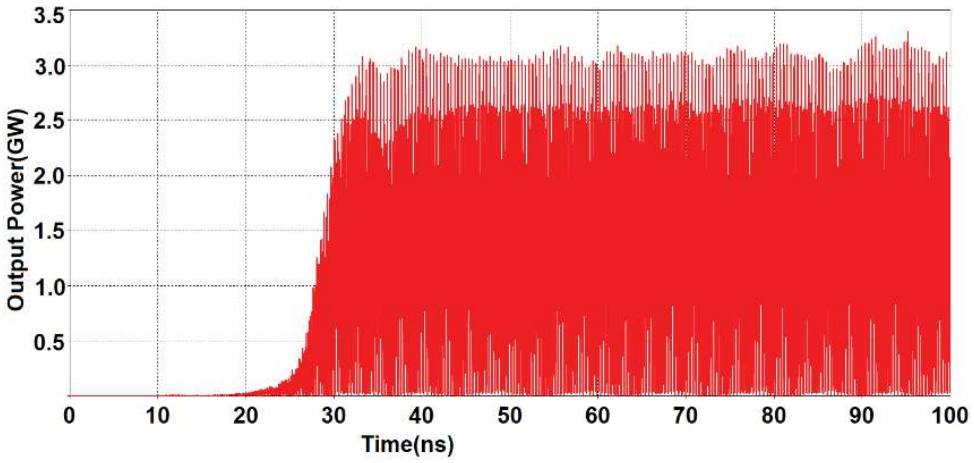

Fig. 3.16: Peak output power of the MILO [[Cousin *et al.* (2007)] obtained through CST simulation.

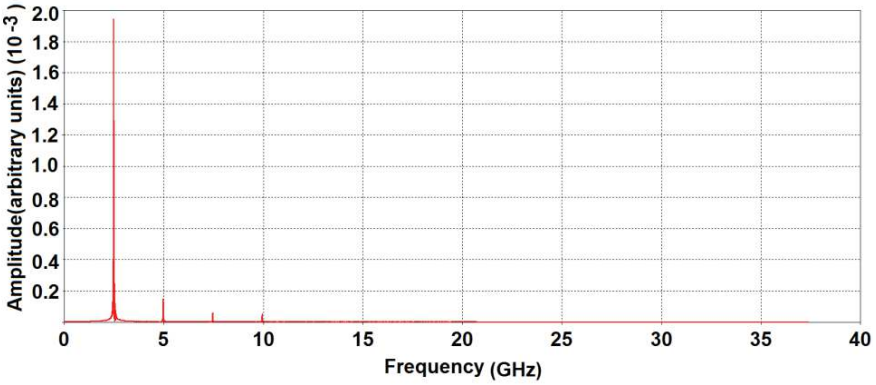

Fig. 3.17. Fourier transform of the electric field at the output port of the MILO [Cousin *et al.* (2007)] obtained through CST simulation.

3.6. Conclusion

In this chapter, an improved S-band MILO has been designed using analytical formulation, simulated by introducing the electron beam in the RF interaction structure and optimized using 3-D electromagnetic PIC code. Further, the beam absent (cold) simulation is carried out for getting the pi-mode operation and pi-mode frequency is arrived at from dispersion characteristics that is obtained using equivalent circuit approach. During the hot simulation Beam-wave interaction phenomena was studied. By employing phase space monitor in simulation helps in monitoring at different instant of time energy transfer phenomena to RF and mechanisms of spoke formation along interaction length of the electromagnetic structure. A set of design parameters have been optimized for enhancement of conversion efficiency that includes reduction in length of cathode and beam dump, inner radii of choke and SWS vane, and placement of stubs. Reducing the length of cathode could manifest several advantages: (i) additional electrons are available for interaction with the desired operating mode for enhanced efficiency (i. e., higher number of spoke electrons could participate in interaction), (ii) sufficient self-generation of magnetic field, and (iii) the reduced cathode length prevents cantilever axial shift and off-axis asymmetric emission of

electron beam. The peak power of 6 GW and a frequency of 3.1 GHz at TM_{01}-mode with power conversion efficiency of ~25% have been achieved with the diode voltage of 500 kV and current of 47.5kA. Also the performance and improvement in MILO structure during beam-wave interaction mechanisms has been carried out. Thus the total length of the MILO has been significantly reduced by ~22% as compared to the earlier conventional MILO.

In order to validate the efficacy of the present analysis using CST Particle Studio, validation exercise has been carried out against a model of the device for which the details were available in the literature [Cousin *et al.* (2007)]. A comparison of the results has been tabulated as Table 3.2. Typical simulated peak output power and Fourier Transform of the electric field at the output port of MILO [Cousin *et al.* (2007)] have been shown in Figs. 3.16 and 3.17, respectively.